



A New Way for Walén Test of Alfvénic Fluctuations in Solar Wind Streams via EEMD

Jin Liu^{1,2}, ChuanBing Wang^{2,3}, PengYu Wang¹, Dan Du⁴, Xiang Li¹, and GuoQi Liu¹¹ School of Earth Science, Yunnan University, Yunnan 650091, People's Republic of China; liuj3268@ustc.edu.cn² CAS Key Laboratory of Geospace Environment, School of Earth and Space Sciences, University of Science and Technology of China, USTC, Anhui 230026, People's Republic of China; cbwang@ustc.edu.cn³ CAS Center for the Excellence in Comparative Planetology, Hefei, Anhui 230026, People's Republic of China⁴ Key Laboratory of Space Weather, National Center for Space Weather, China Meteorological Administration, Beijing 100081, People's Republic of China

Received 2019 December 28; revised 2020 January 28; accepted 2020 January 29; published 2020 March 16

Abstract

Pure Alfvén waves at 1 au can be effectively identified by a Walén test of plasma and magnetic field observations. In this study, a new method, based on the Ensemble Empirical Mode Decomposition (EEMD) technique, is proposed for analyzing Alfvén fluctuations in two ways: (1) the Walén test relied on a time-dependent frame, which is extracted from the trend of differences between plasma and Alfvén velocity; and (2) a modified Walén test of the reconstructed Alfvénic and plasma velocity fluctuations by EEMD, after removing the high/low-frequency components irrelevant to Alfvénicity. Referencing the three validated methods mentioned in Chao et al., the same four cases in high-speed solar wind streams are tested by the EEMD method, considering Alfvénic parameters such as the Walén slope, the standard deviation ratio, the Alfvén ratio, the normalized cross helicity, the normalized residual energy, and the mean deviation relative to 1. The test results indicate that the first EEMD method can improve most Alfvénic parameters, since a time-varying velocity of the De Hoffmann–Teller frame is obtained from the process of self-adaptive data analysis, especially for complex cases with nonstationary and multiple background frames. The second EEMD method provides a kind of flexible testing to reconstruct the optimal fluctuations satisfied for the Walén relation, which achieves similar or even better results than normal prior methods based on bandpass filtering. We suggest that the EEMD method can be an alternative way to identify large-amplitude Alfvén waves in solar wind streams with single-satellite data.

Unified Astronomy Thesaurus concepts: Alfvén waves (23); Solar wind (1534); Magnetohydrodynamics (1964); Interplanetary magnetic fields (824); Space plasmas (1544)

1. Introduction

Since Alfvén waves (Alfvén 1947) in interplanetary space were observed by *Mariner 2* during their flights to Venus in the 1960s (Barnes et al. 1962), many Alfvén fluctuations (AFs) have been found in the solar atmosphere and solar wind, especially in high-speed streams (De Pontieu et al. 2007; Tomczyk et al. 2007; He et al. 2009; Wang et al. 2012; Yang et al. 2016; Martínez-Sykora et al. 2017). According to the observation statistics of *Mariner 5*, large-amplitude Alfvén waves account for 30% of the solar wind fluctuations at least (Coleman 1967; Belcher et al. 1969). It is believed that Alfvén waves could contribute to energy transmission and dissipation in phenomena as solar corona heating, solar wind acceleration, and geomagnetic disturbances (Alazraki & Couturier 1971; Wentzel 1974; Jacques 1977; Tsurutani & Gonzalez 1987; Matthaeus et al. 1999; McIntosh et al. 2011; Wang et al. 2014). Generally, Alfvén waves can be recognized by the strong correlation between fluctuations of magnetic field \mathbf{B} and plasma velocity \mathbf{V} from in situ measurements of the solar wind (Unti & Neugebauer 1968), and most of these fluctuations are considered outward propagating Alfvén waves originating near or at the Sun (Belcher et al. 1971). It is also observed that large-amplitude Alfvén waves (relative to the magnitude of the ambient magnetic field \mathbf{B}_0) frequently occurred at the trailing edge of high-speed streams, with multiscale fluctuations

varying from several minutes to a few hours (Bruno et al. 1985; Mavromichalaki et al. 1988).

Under the hypothesis of constant plasma density, thermal pressure, and magnetic field strength, according to the ideal MHD theory, for Alfvén waves correlated fluctuations of plasma velocity and magnetic field satisfy the Walén relation (Walén 1944; Belcher et al. 1969; Hudson 1971; Barnes & Hollweg 1974; Yang & Chao 2013)

$$V_{\perp} = \pm \xi^{1/2} [B_{\perp} / (\mu_0 \rho)^{1/2}] + \text{const.} \quad (1)$$

Here, V_{\perp} and B_{\perp} are the plasma velocity and magnetic field component perpendicular to both the background magnetic field \mathbf{B}_0 and wave vector \mathbf{k} , ρ is the plasma density, and μ_0 is the permeability in vacuum; the “+/-” sign represents waves propagating antiparallel/parallel to \mathbf{B}_0 . ξ is the thermal anisotropic parameter given by

$$\xi = 1 - \frac{P_{\parallel} - P_{\perp}}{B_0^2 / \mu_0}, \quad (2)$$

where P_{\parallel} and P_{\perp} are the thermal pressure parallel and perpendicular to \mathbf{B}_0 , respectively. The values of ξ was published in the range from 0.8 to 1.0 considering the anisotropies of protons and electrons (Burlaga 1971). Corrections between 4% and 7% follow from the total anisotropies measured on *Helios* near 1 au (Marsch & Richter 1984).

If the solar wind plasma is assumed to be incompressible, the magnetic field and velocity perturbations $\delta \mathbf{B}$ and $\delta \mathbf{V}$ are related



Original content from this work may be used under the terms of the [Creative Commons Attribution 4.0 licence](https://creativecommons.org/licenses/by/4.0/). Any further distribution of this work must maintain attribution to the author(s) and the title of the work, journal citation and DOI.

through (Wu 1995)

$$\delta \mathbf{V} / V_A = \pm \delta \mathbf{B} / B_0, \quad (3)$$

where V_A is the local Alfvén velocity in anisotropic media:

$$V_A \equiv \xi^{1/2} \frac{B_0}{(\mu_0 \rho)^{1/2}}. \quad (4)$$

Both Equations (1) and (3) represent the theoretical relation. In practice, the observed fluctuations of \mathbf{B} and \mathbf{V} represent the temporal variations relative to satellites, which actually include some uncertainties unrelated to Alfvén waves. As mentioned above, the remarkable feature of Alfvén waves is that perturbations of plasma velocity and magnetic field are parallel and proportional to each other. Therefore, when it refers to identify Alfvén waves, the simplified Walén relation is tested by a linear fitting between data of plasma and Alfvén velocities for a certain period of time, as a criterion for the degree of Alfvénicity, the so-called Walén test. Meanwhile, appropriate methods are necessary for processing and analyzing the observation data to eliminate the uncertainties unrelated to Alfvén waves, particularly for single-spacecraft measurements.

The conventional method for Walén tests depends on a stationary De Hoffmann–Teller frame (hereafter referred to as the HT frame), which was originally defined by De Hoffmann & Teller (1950) while analyzing the conditions across a one-dimensional MHD shock boundary. If a real HT frame exists, or as a reasonable approximation, there is a quasi-stationary pattern, where the magnetic field and the plasma velocity are highly coherent, such as a wave or a current layer. That is, the plasma flows through the shock wave or current layer in the field direction, and the normal component of the HT frame velocity represents the motion of an entire layered structure (Paschmann & Daly 2000). Since the observed plasma velocity \mathbf{V} in the instrument frame are composed of the HT frame velocity \mathbf{V}_{HT} , the plasma velocity in HT frame \mathbf{V}' , and other uncertainty \mathbf{V}_u (Chao et al. 2014), the HT analysis is an assessment of the uncertainty margins of the HT velocity vector using the minimization procedure. To approximate the \mathbf{V}_{HT} from measurements of \mathbf{B} and \mathbf{V} in a concerned time interval, the common method is to minimize the residual electric field by the minimum variance analysis (MVA; Sonnerup & Cahill 1967), the so-called MVA method. That is, we calculate the convective electric field \mathbf{E} ($= -\mathbf{V} \times \mathbf{B}$) using the magnetic field and the plasma velocity in the HT frame, namely

$$D = \frac{1}{T} \sum_{t=1}^T |(\mathbf{V}' - \mathbf{V}_{HT}) \times \mathbf{B}'|^2 \quad (5)$$

In principle, any non-negative merit function can be used to find the best fit for \mathbf{V}_{HT} evolution. By solving the conditions $\partial D / \partial \mathbf{V}_{HT} = 0$, we can get \mathbf{V}_{HT} when D (or \mathbf{E}) is minimum, where D is defined as Equation (5) and the superscript t is used to denote the T individual data points in the operation $\frac{1}{T} \sum_{t=1}^T$ (Sonnerup et al. 1987). The Walén slope is defined as the ratio of V'_i / V_{Ai} using a least-squares fitting technique (Khrabrov & Sonnerup 1998). Here V'_i and V_{Ai} are the i th plasma and Alfvén velocity component ($i = x, y, z$) in the HT frame, respectively. When the Walén slope is close to 1, with a strong correlation (correlation coefficient ≈ 1) between plasma velocity and magnetic field, a pure Alfvén wave is qualified. The Walén

Table 1
Alfvén Wave Events and Related Parameters

Case No.	Date	Start (UT)	End (UT)	Duration
Case 1.	1995 Jan 29	20:20	20:55	35 minutes
Case 2.	1995 Feb 3	09:00	10:00	60 minutes
Case 3.	2002 Oct 14	18:16	18:52	36 minutes
Case 4.	2002 Oct 17	17:40	22:00	140 minutes

Note. The parameters are listed in the following format: observation date (yyyymmdd), start time (hh:mm), end time (hh:mm). These events are selected from Chao et al. (2014).

relation can be simplified as

$$V'_i = \pm V_{Ai}. \quad (6)$$

In an HT frame, if the magnetic field structures sampled are stationary, the motional electric field vanishes, and purely Alfvénic fluctuations qualify the Walén test well. However, sometimes the Walén slope is quite sensitive to the concerned time period because the MVA technique depends on sampled data segments with an unacceptable relative difference (Jensen et al. 2013).

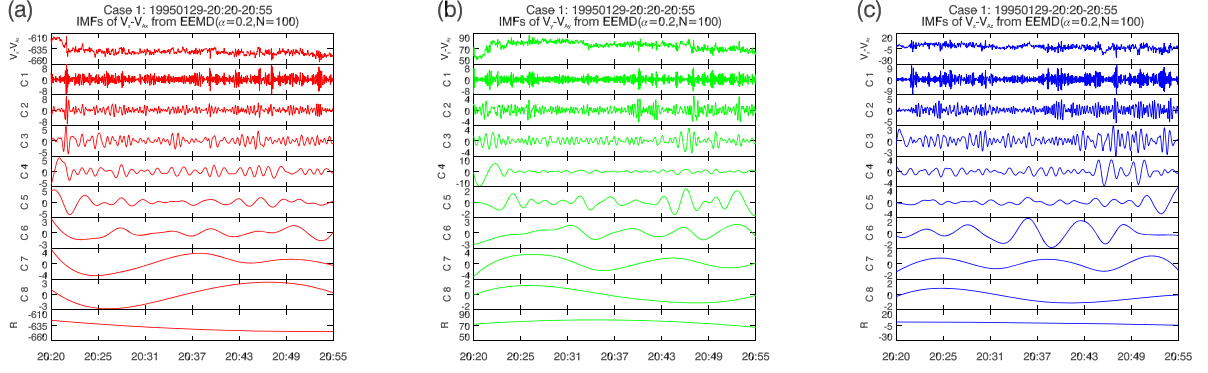
As an alternative method, one can estimate the HT frame using another method, in which each component of \mathbf{V}_{HT} is calculated from average deviations of the components of solar wind plasma velocity V_i and Alfvén velocity V_{Ai} as Equation (7) (Chao et al. 2014), so we call it the mean deviation method. The slopes of x, y, z components are likely to be quite different, so it is considered less credible to evaluate the Walén relation depending on an average of the three component slopes.

$$V_{HTi} = \frac{1}{T} \sum_T (V_i - V_{Ai}). \quad (7)$$

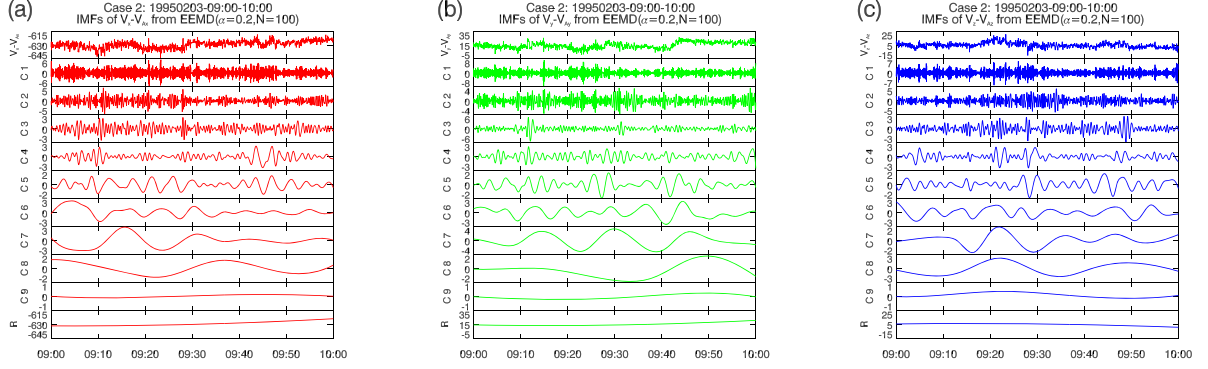
Similar \mathbf{V}_{HT} and averaged slopes were obtained from the above two methods for the four cases in Chao et al. (2014), identifying the pure large-amplitude Alfvén waves in stationary HT frames. However, it is difficult to find an HT frame when some time-independent structures exist, particularly as a perpendicular structure with a strong intrinsic electric field (Paschmann & Daly 2000). The slopes from the conventional methods are not always credible because the HT frame may change in practice, such as in nonuniform high-speed streams occupied by multiscale dynamic structures. In such cases, the electric field in the constant HT frame does not vanish and the Walén test in this time segment probably provides an inaccurate indication for Alfvénic fluctuations. Likewise, if the HT frame velocity obtained by the mean deviation method does not coincide with the stationary structure, the assumption of Alfvénic fluctuations in all components relative to average values needs to be reexamined (Gosling et al. 2009). Thus, a practical reference frame is expected from the observed plasma velocity to qualify the AFs containing the motion of current layers, discontinuities or any other nonstationary structures.

Considering the uncertainty from the HT frames, Chao et al. (2014) proposed a modified method (hereafter the CHYL method), to check the Walén relation using time difference data between the neighborhood values of plasma and Alfvén velocities, i.e., $\Delta V^t = V^{t+1} - V^t$ and $\Delta V_A^t = V_A^{t+1} - V_A^t$. Specifically, when the sampling rate is high enough, the time difference data are independent of \mathbf{V}_{HT} and \mathbf{V}_u , which means

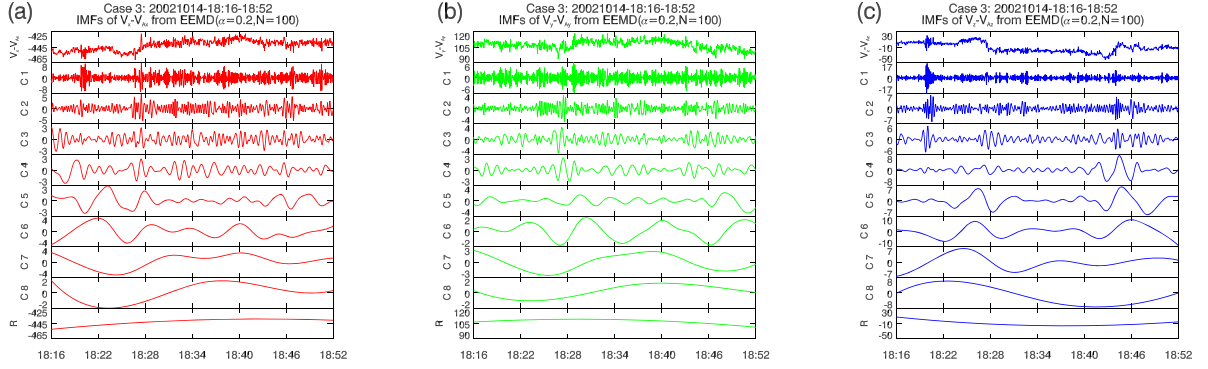
- (A) Case 1



- (B) Case 2



- (C) Case 3



- (D) Case 4

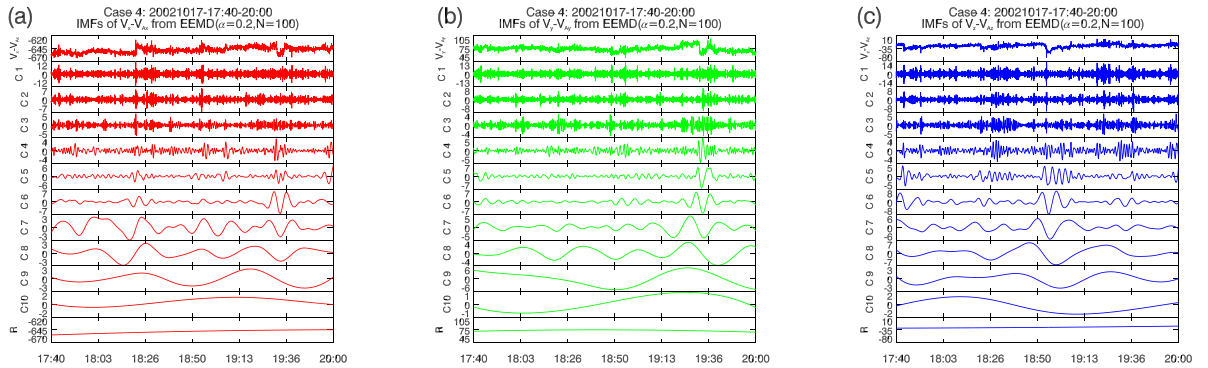


Figure 1. Decomposed IMFs and residual of EEMD from the differences of plasma and Alfvén velocity components. The subfigures (A)–(D) show the results of Cases 1–4, respectively, in which (a)–(c) show the IMF curves of x , y , z components in red, green, and blue, specifically derived from $(V_x - V_{Ax})$, $(V_y - V_{Ay})$, $(V_z - V_{Az})$ in GSE coordinates in units of km s^{-1} , in which the amplitude ratio α of added white noises in each trial is set to a value of 0.2 and the ensemble number $N = 100$.

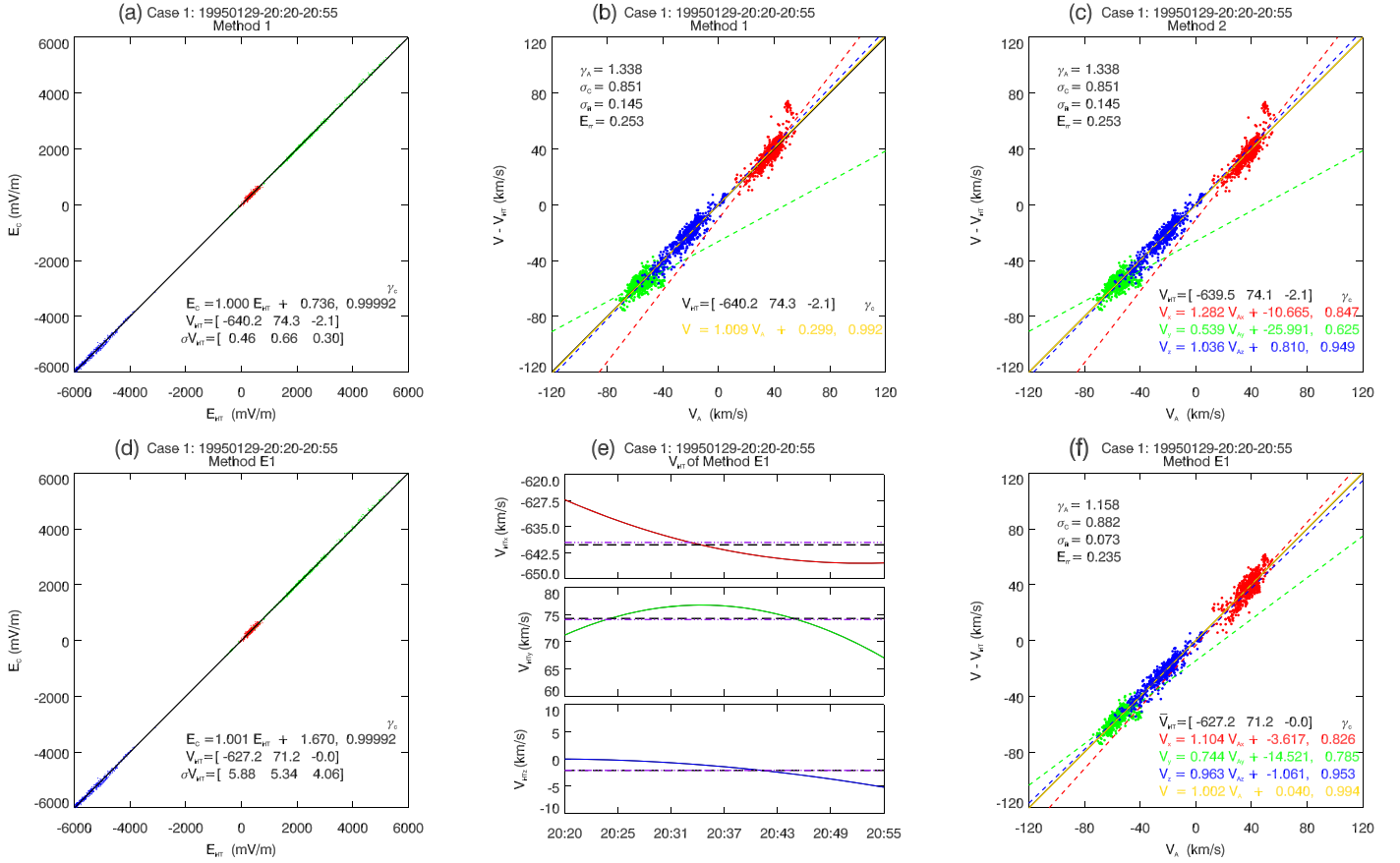


Figure 2. Walén analysis of Case 1. (a) The conformance test of electric field E_c vs. E_{HT} in the HT frame by Method 1. (b) Results of the Walén test from Method 1 showing V' vs. V_A . Red, green, and blue represent the x , y , z components in GSE coordinates, and the dots and lines indicate the original data and their linear fitting results, respectively. The values of HT frame velocity V_{HT} , correlation coefficient γ_c , four additional Alfvénicities (γ_A , σ_c , σ_R , E_{HT}), and linear regression fits are labeled in the figures. (c) The results of the Walén test for the x , y , and z components from Method 2 are in the same format as (b). (d) Test of the electric field E_c vs. E_{HT} from Method E1 in the same format as (a). (e) The HT frame velocity in Method E1 (solid lines), corresponding to the residue of EEMD shown in Figure 1. Here the dotted-dashed and dashed lines show the HT frame velocity in Method 1 and 2, respectively. (f) Results of the Walén test from Method E1 in the same format as (b) and (c), in which the label of V_{HT} is the average velocity over the selected period of time.

Table 2
Alfvénic Parameters for the Walén Test of Case 1

Parameter		$\gamma_c \frac{\sigma V'_i}{\sigma V_{Ai}}$	γ_c	$\frac{\sigma V'_i}{\sigma V_{Ai}}$
V' versus V_A	Method 1	1.009	0.992	1.017
	Method E1	1.002	0.994	1.008
V_x versus V_{Ax}	Method 2	1.282	0.847	1.514
	Method E1	1.104	0.826	1.337
V_y versus V_{Ay}	Method 2	0.539	0.625	0.862
	Method E1	0.744	0.785	0.948
V_z versus V_{Az}	Method 2	1.036	0.949	1.092
	Method E1	0.963	0.953	1.010

these velocities can be assumed as constant during the period, so $\Delta V(j) = \Delta V'(j)$. Then the Walén relation can be modified as

$$\Delta V' = \pm \Delta V_A \quad \text{or} \quad \Delta V = \pm \Delta V_A. \quad (8)$$

Because time difference data can magnify the values of noises derived from the high-frequency components of an original observation, the values of plasma and Alfvén velocities need to be smoothed by a low-pass filter before generating the difference data in the modified Walén test. This implies that we

must preset the frequency range for a bandpass filter without knowing whether the filtered part has an Alfvénic nature. The advantage of this method is that it provides a way to test the Walén relation without relying on any HT frames. But it reduced the original correlation between the plasma velocity V and Alfvénic velocity V_A more or less, as seen in the actual results of Chao et al. (2014). Afterward, a new approach was proposed in Li et al. (2016) to check the Walén relation using the multiple-bandpass filtered data instead of the difference data sets.

Considering the multiscale and nonstationary properties of the background streams, a self-adaptive decomposing technique, the Ensemble Empirical Mode Decomposition (EEMD) is applied for the Walén test of Alfvénic fluctuations, and is designed for auxiliary analysis of nonstationary and nonlinear fluctuations. The EEMD technique has recently been applied for numerical and image data, including timescale separation in the solar wind-magnetosphere coupling (Alberti et al. 2017), spectral properties of solar wind density fluctuations (Carbone et al. 2018), temperature variation of sea surfaces (Carbone et al. 2016b), and geophysical turbulences in oceanic environments (Carbone et al. 2016a). In this paper, we find that EEMD can help us remove the irrelevant Alfvénic components from the observation and improve the performance of the Walén test.

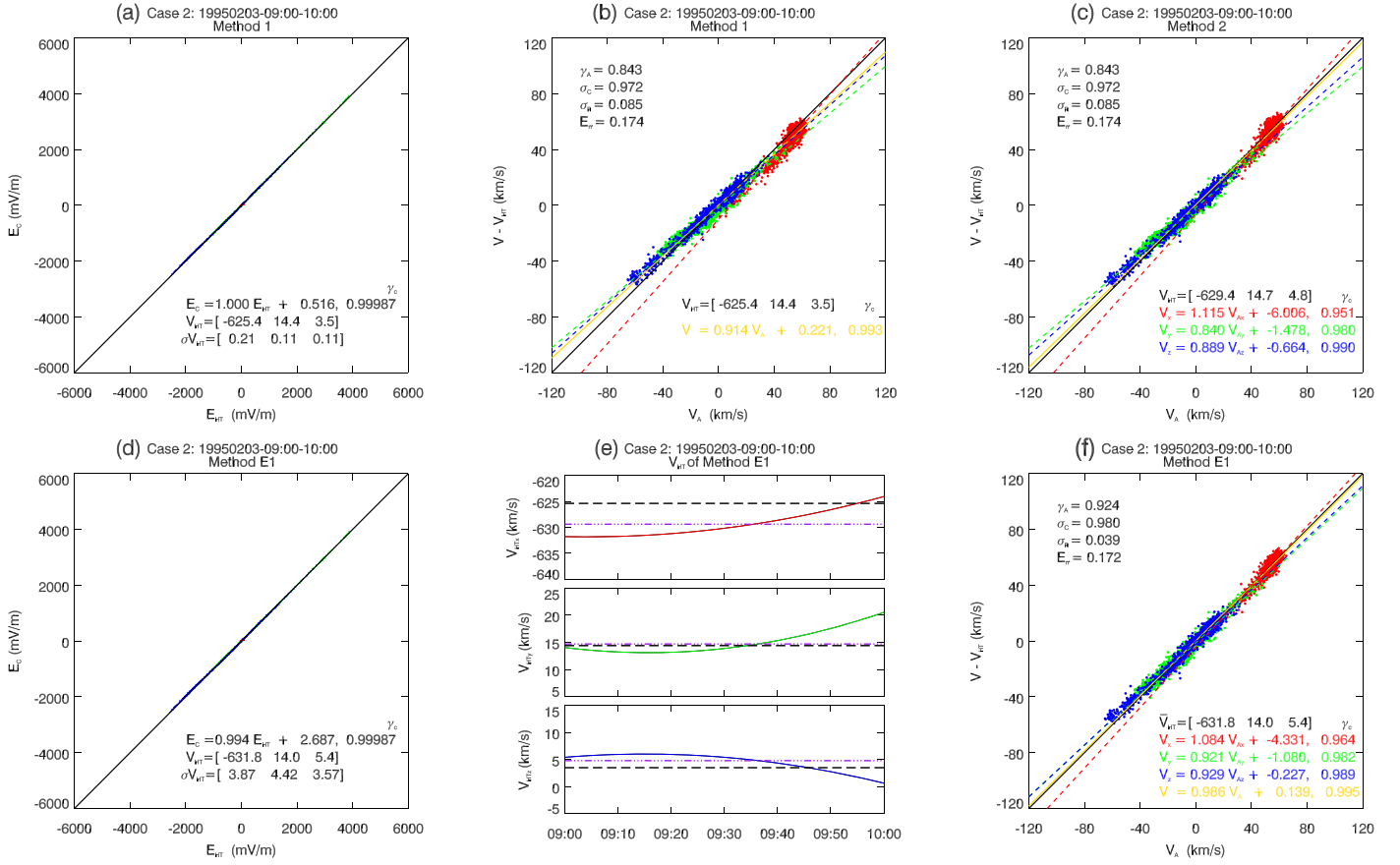


Figure 3. Walén test results of Case 2 in the same format as Figure 2.

Table 3

Alfvénic Parameters for the Walén Test of Case 2

Parameter		$\gamma_c \frac{\sigma V_l'}{\sigma V_{Ai}}$	γ_c	$\frac{\sigma V_l'}{\sigma V_{Ai}}$
V' versus V_A	Method 1	0.914	0.993	0.920
	Method E1	0.986	0.995	0.991
V_x versus V_{Ax}	Method 2	1.115	0.951	1.172
	Method E1	1.084	0.964	1.124
V_y versus V_{Ay}	Method 2	0.840	0.980	0.857
	Method E1	0.921	0.982	0.938
V_z versus V_{Az}	Method 2	0.889	0.990	0.898
	Method E1	0.929	0.989	0.939

This paper is organized as follows. In Section 2, the decomposition procedures of EEMD and the Alfvénic parameters used in this work are introduced. In Section 3, four Alfvén wave events observed by *WIND* are tested by the EEMD method and other methods for comparison, considering the Alfvénic parameters described in the Section 2.2. Sections 4 and 5 are the discussion and conclusion, respectively.

2. Methodology

2.1. EEMD

The time-frequency data analysis technique known as Hilbert–Huang Transform (HHT) was proposed by Huang et al. (1998a), and is widely used to process various nonlinear

and nonstationary data. It consists of two parts: Empirical Mode Decomposition (EMD) and Hilbert spectral analysis (HSA; Huang et al. 2008).

Unlike traditional time-frequency methods like the Fourier transform and wavelets, HHT is not based on a priori harmonic functions. Instead, it is based on the essential characteristics of the data without setting any basis function. We can use EMD to decompose complex signals into a series of Intrinsic Mode Functions (IMFs) and a monotonous residual naturally (Huang et al. 1998b). The self-adaptive decomposition ensures that the IMFs retain enough physical essence like the amplitude and frequency of the original signals. However, there are some defects of EMD, such as mode mixing, a lack of physical uniqueness and robustness when it is applied to noisy data. As an extended version of EMD, EEMD is a noise-assisted data analysis method developed by Wu & Huang (2004) to overcome the above problems.

The data processing by EEMD is carried out as follows: first, finite-amplitude white noises are added to the original signal as a whole; second, decomposed signals with added white noises go into IMFs according to EMD; then, repeat the above processes for many trials with different random white noises each time; finally, obtain the (ensemble) means of corresponding IMFs. On account of the statistical characteristics of the Gaussian white noise mean value of zero, the final IMFs avoid the influence of adding noises through multiple sets of average processing. Taking the time-series signal as an example, $V_z(t)$ represents a component of plasma or Alfvén velocity, which

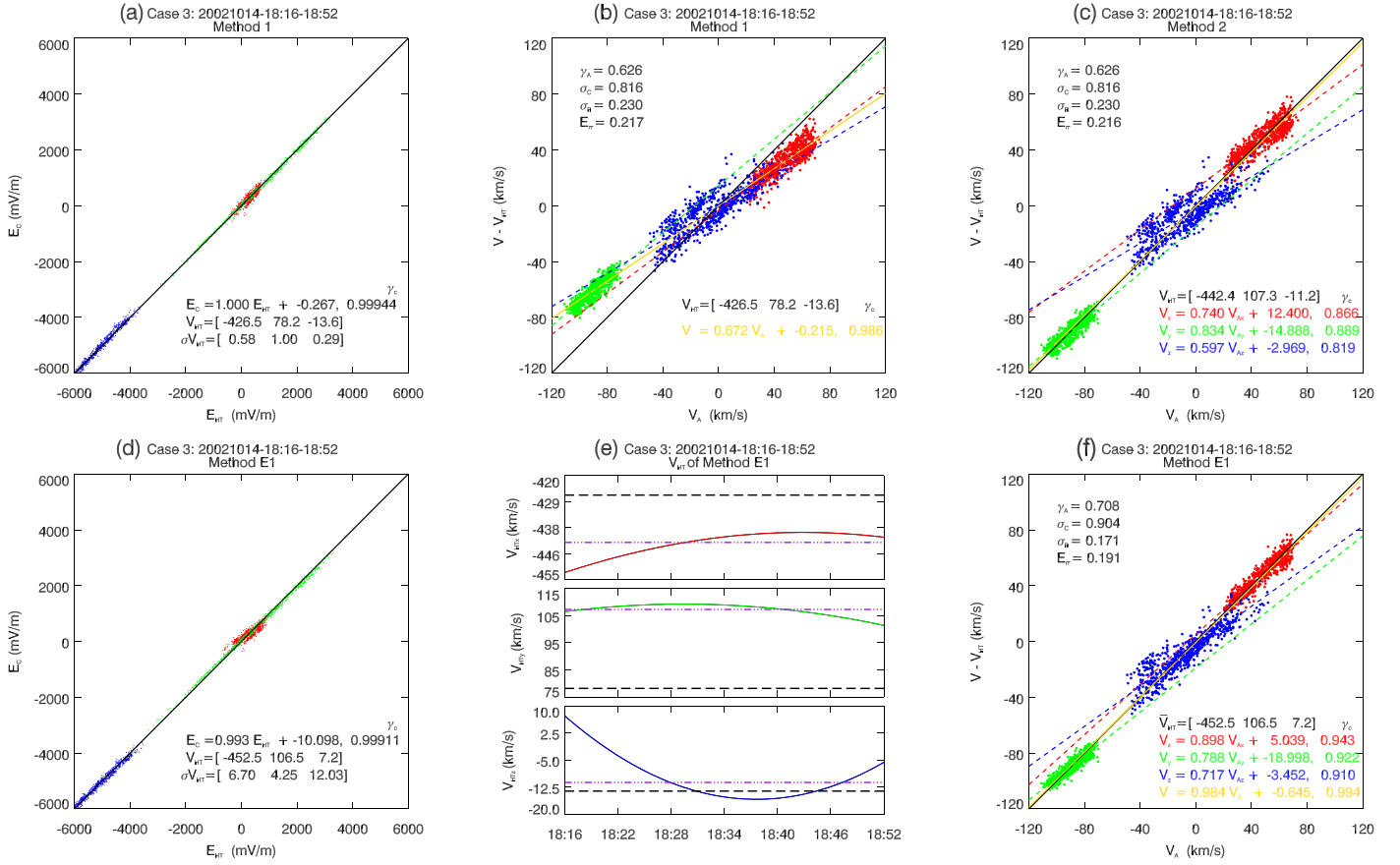


Figure 4. Walén test results of Case 3 in the same format as Figure 2.

Table 4
Alfvénic Parameters for the Walén test of Case 3

Parameter		$\gamma_c \frac{\sigma V'_l}{\sigma V_{Ai}}$	γ_c	$\frac{\sigma V'_l}{\sigma V_{Ai}}$
V' versus V_A	Method 1	0.672	0.986	0.682
	Method E1	0.984	0.994	0.990
V_x versus V_{Ax}	Method 2	0.740	0.866	0.855
	Method E1	0.898	0.943	0.952
V_y versus V_{Ay}	Method 2	0.834	0.889	0.938
	Method E1	0.788	0.922	0.855
V_z versus V_{Az}	Method 2	0.597	0.819	0.729
	Method E1	0.717	0.910	0.788

can be decomposed in terms of a group of IMFs, i.e.,

$$V_i(t) = \sum_{k=1}^n C_k(t) + R_n, \quad (9)$$

where R_n is the residue of $V_i(t)$ after n IMFs being extracted, the $C_k(t)$ is the k th IMF defined by EEMD as follows:

$$C_k(t) = \lim_{N \rightarrow \infty} \frac{1}{N} \sum_{l=1}^N [C_{k,l}(t) + \alpha R_l(t)] \quad (10)$$

As the ensemble number N tends to be infinite, $C_{k,l}(t) + \alpha R_l(t)$ is the portion of the l th trial in the k th IMF in the noise-added signal, with amplitude percentage α as the added noise in each

ensemble member versus the original data. In the EMD procedure, to keep the program from going on infinitely, there is a normal criterion for the EMD process to stop: the standard deviation (SD) is computed from the two consecutive sifting results (Huang et al. 2008). The SD is usually set to the value between 0.1 and 0.3, with the same value as α in the procedure.

In this study, EEMD is applied for the Walén test in two ways. The first EEMD method is to extract the HT frame velocity from the decomposed results of plasma and Alfvén velocity difference $V_i - V_{Ai}$. The second EEMD method is to test Walén slopes using the reconstructed fluctuations of V and V_A , which are combinations of IMFs decomposed by EEMD.

2.2. Alfvénic Parameters

In different forms, such as Equations (1), (2), (6), and (8), the Walén relation is always the primary criterion for Alfvénic fluctuations. In addition, there are several approved Alfvénic parameters that can be used to estimate if an Alfvén wave exists or the degree of Alfvénicity.

(1) The correlation coefficient γ_c and the slope of V' versus V_A are primary parameters for identifying Alfvén waves in solar wind. Usually, a linear regression through the origin is recommended to meet the Walén slope (Eisenhauer 2003).

(2) The ratios of SDs of all the components of plasma velocity to Alfvén velocity fluctuations are calculated as $\sigma_{V'}/\sigma_{V_A}$ or $\sigma_{\Delta V'}/\sigma_{\Delta V_A}$ (Chao et al. 2014), reflecting the relative SDs of velocity and magnetic field signals. The correlation coefficient corrected by the ratio of standard variance is equal

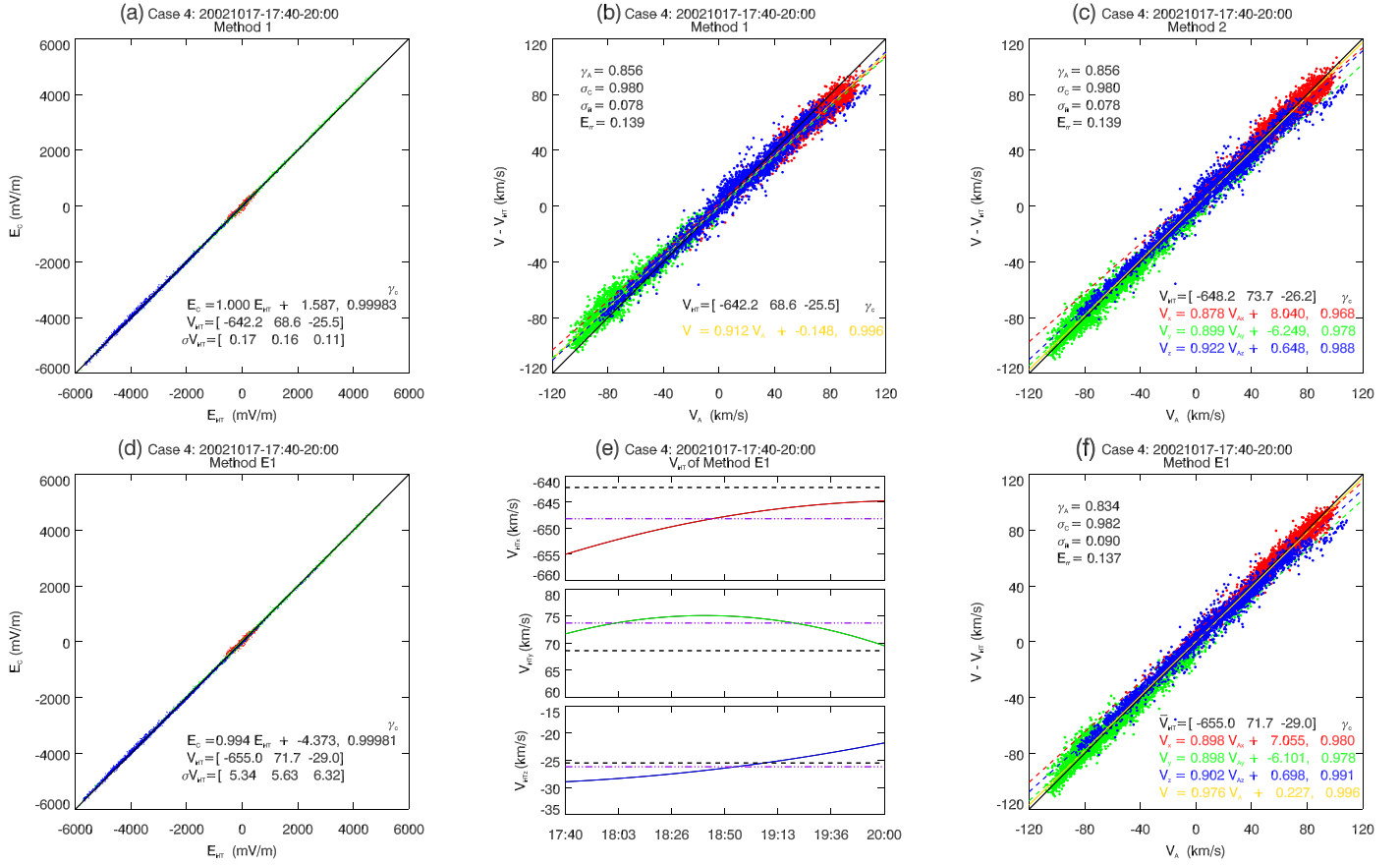


Figure 5. Walén test results of Case 4 in the same format as Figure 2.

Table 5
Alfvénic Parameters for the Walén Test of Case 4

Parameter		$\gamma_c \frac{\sigma V'_i}{\sigma V_{Ai}}$	γ_c	$\frac{\sigma V'_i}{\sigma V_{Ai}}$
V' versus V_A	Method 1	0.912	0.996	0.916
	Method E1	0.976	0.996	0.980
V_x versus V_{Ax}	Method 2	0.878	0.968	0.907
	Method E1	0.898	0.980	0.916
V_y versus V_{Ay}	Method 2	0.899	0.978	0.919
	Method E1	0.898	0.978	0.918
V_z versus V_{Az}	Method 2	0.922	0.988	0.933
	Method E1	0.902	0.991	0.910

to the Walén slope from the linear regression fits, exactly as

$$\gamma_c \frac{\sigma'_V}{\sigma V_A} \quad \text{or} \quad \gamma_c \frac{\sigma_{\Delta V'}}{\sigma_{\Delta V_A}}.$$

(3) The Alfvén ratio is defined as

$$\gamma_A = \langle \delta V^2 \rangle / \langle \delta V_A^2 \rangle. \quad (11)$$

This indicates the ratio between the kinetic energy density in the plasma frame and the magnetic energy density of the plasma fluctuations (Tu & Marsch 1995). In Equation (11), δV is the plasma velocity fluctuation vector estimated as $\delta V = V' - \langle V \rangle$, and δV_A is the Alfvén velocity fluctuation vector estimated as $\delta V_A = V'_A - \langle V_A \rangle$, where the bracket denotes the average on the time domain.

(4) The normalized cross helicity is σ_c is defined by Matthaeus & Goldstein (1982) as

$$\sigma_c = 2 \langle \delta V \cdot \delta V_A \rangle / (\langle \delta V^2 \rangle + \langle \delta V_A^2 \rangle). \quad (12)$$

If the above parameters are close to 1 or -1 , it is believed that a pure Alfvén wave exists in the plasma velocity and magnetic field fluctuations in nature.

(5) The normalized residual energy σ_R (Yokoi & Hamba 2007) is calculated from

$$\sigma_R = (\langle \delta V^2 \rangle - \langle \delta V_A^2 \rangle) / (\langle \delta V^2 \rangle + \langle \delta V_A^2 \rangle). \quad (13)$$

(6) As a stricter parameter, Li et al. (2016) defines E_{tr} , the mean of SD ratios relative to 1 together with the correlation coefficient between plasma velocity and Alfvén velocity fluctuation:

$$E_{\text{tr}} = \left\langle \left| |\gamma_c| - 1 \right|, \left| |\gamma_{ci}| - 1 \right|, \left| \frac{\sigma_{\delta V}}{\sigma_{\delta V_A}} - 1 \right|, \left| \frac{\sigma_{\delta V_i}}{\sigma_{\delta V_{Ai}}} - 1 \right| \right\rangle \quad (i = x, y, z). \quad (14)$$

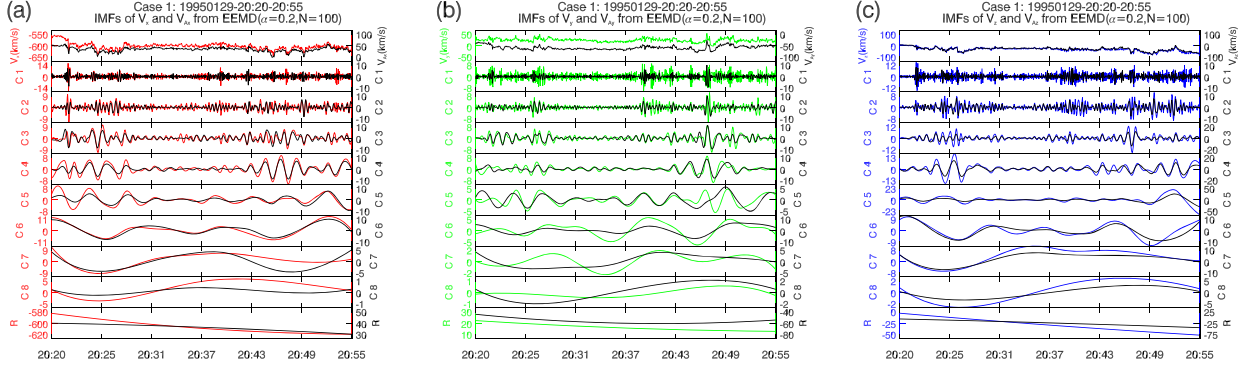
In Equations (13) and (14), the closer σ_R and E_{tr} are to zero, the better the Walén relations are satisfied.

3. Data and Analyses

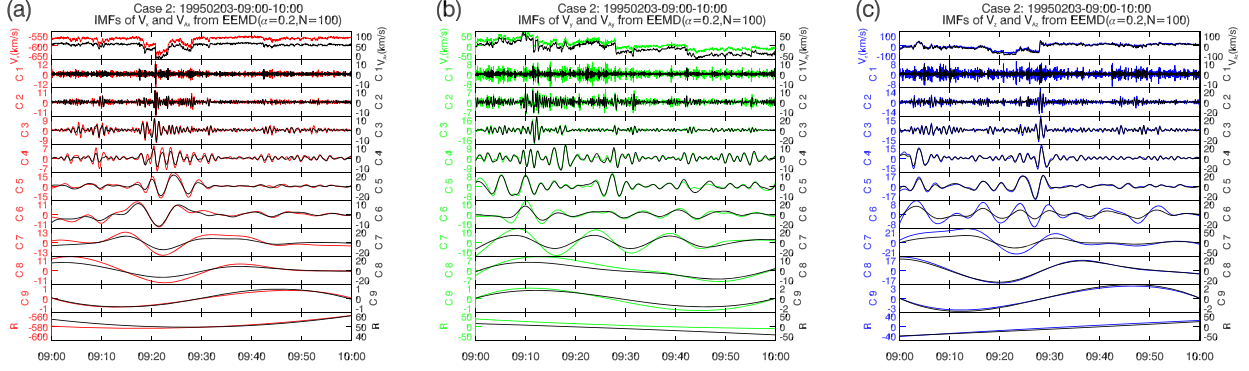
3.1. Alfvén Waves Cases

Observations of magnetic field and plasma velocities are necessary to search for Alfvén wave events in interplanetary

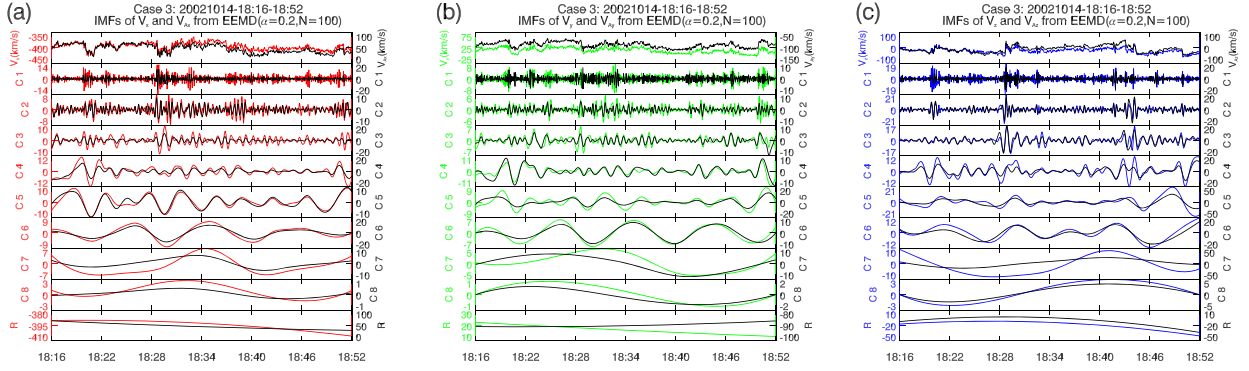
- (A) Case 1



- (B) Case 2



- (C) Case 3



- (D) Case 4

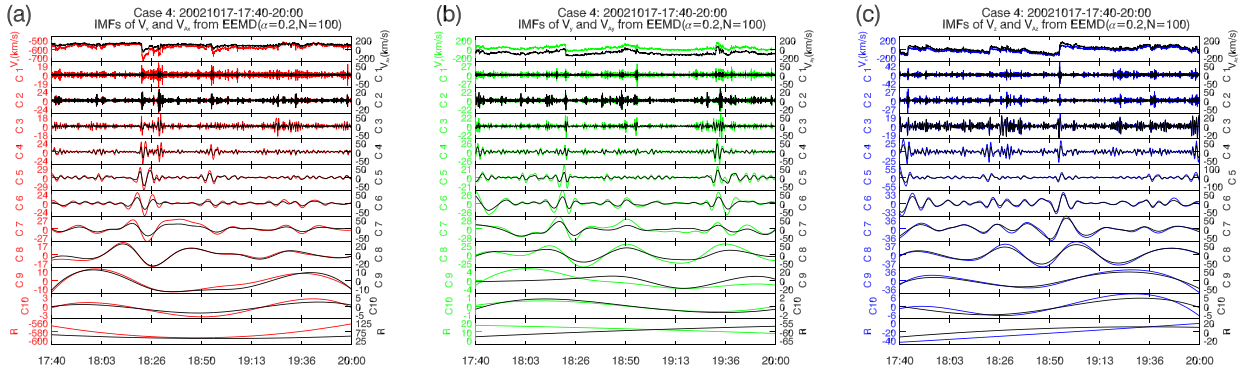


Figure 6. Decomposition results of EEMD from velocity components. The panels present corresponding plasma (red, green, blue) and Alfvén (black) velocity components in the same coordinate, specifically represented as V_x vs. V_{Ax} , V_y vs. V_{Ay} , V_z vs. V_{Az} in GSE coordinates, in which the added white noise has an amplitude ratio of 0.2 and the ensemble number $N = 100$. The subfigures (A)–(D) show the result of Cases 1–4, respectively.

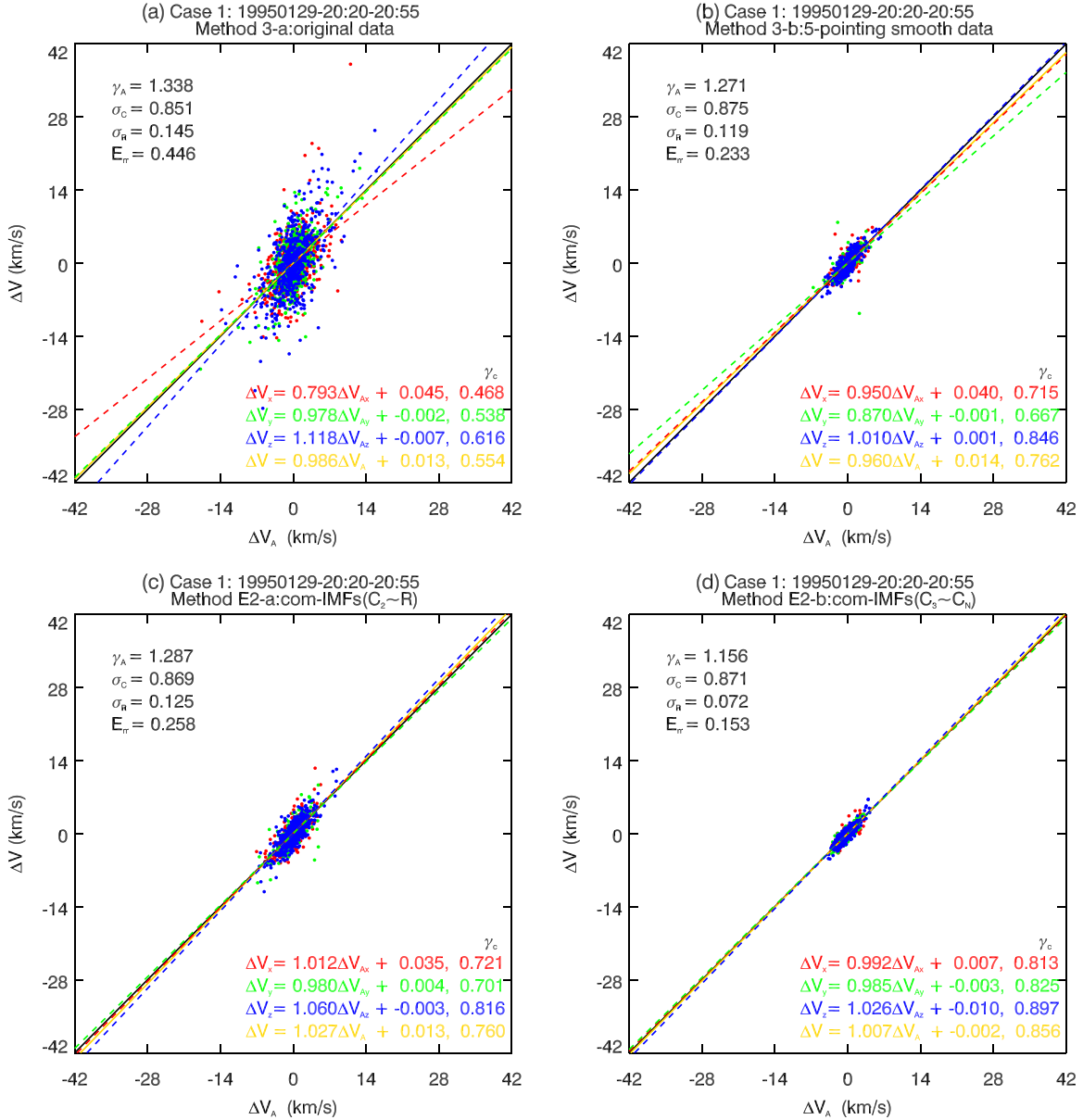


Figure 7. Modified Walén test results of Case 1. (a) The linear regression fitting for ΔV vs. ΔV_A from Method 3-a. (b) Results of five-point running averaged data in Method 3-b with the same format as (a). (c) and (d) show the results from Method E2 in the same format as (a), based on the group of IMFs $C_2 \sim R$ and $C_3 \sim C_N$, correspondingly. The value of the correlation coefficient γ_c , four additional Alfvénicities (γ_A , σ_c , σ_R , E_π), and a linear regression fit are also labeled in the figure.

space and further analyze their properties. The interplanetary magnetic field and solar wind plasma data in this paper are obtained from the Three-dimensional Plasma and Energetic Particle (3DP; Lin et al. 1995) and the Magnetic Field Investigation (MFI) (Lepping et al. 1995) on board the *WIND* spacecraft, with about a 3 s time resolution in geocentric solar ecliptic (GSE) coordinates. The plasma density and velocity are estimated as the contribution of proton and helium, without the electron flow velocity.

In order to compare the results of the EEMD method with other approaches, we choose the same four cases of Chao et al. (2014), as shown in Table 1. These four typical cases are selected as large-amplitude Alfvénic fluctuations during high-speed solar wind streams. Case 1 and Case 3 are observed in the leading portion of a stream where the magnetic field B_t and plasma density N_p are enhanced, while Case 2 and Case 4 are observed at the trailing portion. The four cases occur during the

period of a solar wind stream where the magnetic field strength and proton number density are almost uniform.

3.2. Walén Test Based on an HT Frame

In this section, three methods are used to evaluate the HT frame velocity and test the conventional Walén relation: the MVA method (Method 1), the mean deviation method (Method 2) and the first EEMD method (Method E1), respectively. For Method 1, the HT frame velocity is satisfied with a minimal residual electric field. For Method 2, the averages of differences between the Alfvén and the plasma velocity components are assumed to be the velocity of the HT frame, as given by Equation (7). For Method E1, the EEMD as a filter allows us to find a nonharmonic trend (residue of EEMD) from the differences between V_i and V_{Ai} that is evaluated as the HT frame velocity.

Table 6
Alfvénic Parameters for the Modified Walén test of Case 1

Parameter		$\gamma_c \frac{\sigma \Delta V_i}{\sigma \Delta V_{Ai}}$	γ_c	$\frac{\sigma \Delta V_i}{\sigma \Delta V_{Ai}}$
ΔV versus ΔV_A	Method 3-a	0.986	0.554	1.780
	Method 3-b	0.960	0.762	1.260
	Method E2-a	1.027	0.760	1.351
	Method E2-b	1.007	0.856	1.176
ΔV_x versus ΔV_{Ax}	Method 3-a	0.793	0.468	1.694
	Method 3-b	0.950	0.715	1.330
	Method E2-a	1.012	0.721	1.404
	Method E2-b	0.992	0.813	1.220
ΔV_y versus ΔV_{Ay}	Method 3-a	0.978	0.538	1.818
	Method 3-b	0.870	0.667	1.304
	Method E2-a	0.980	0.701	1.398
	Method E2-b	0.985	0.825	1.193
ΔV_z versus ΔV_{Az}	Method 3-a	1.118	0.616	1.815
	Method 3-b	1.010	0.846	1.194
	Method E2-a	1.060	0.816	1.299
	Method E2-b	1.026	0.897	1.144

In the process of decomposing the velocity deviation ($V_i - V_{Ai}$) by EEMD, we get a group of IMFs from each component of velocity, and each IMF is the ensemble average of 100 trials ($N = 100$). In each trial, a random white noise is added with the SD of 0.2 ($\alpha = 0.2$). The decomposition results of the above 4 cases are shown in Figure 1, corresponding to curves of original velocity component, all IMFs, and the residue R , respectively. As seen in Figure 1, the number of IMFs obtained from each case is different, $C_1 \sim C_8$ for Case 1 and Case 3, $C_1 \sim C_9$ for Case 2, and $C_1 \sim C_{10}$ for Case 4, which depends on $\log 2(T)$ (Flandrin et al. 2004), where T is the number of data points of original signals.

Case 1 is first taken to demonstrate the test results from the three different methods. By a test $E_c (= -\mathbf{V} \times \mathbf{B})$ versus E_{HT} ($= -\mathbf{V}_{HT} \times \mathbf{B}$), as seen in Figure 2(a), it almost reproduces the result of Chao et al. (2014) by Method 1, evaluating the velocity of HT frame as \mathbf{V}_{HT} : $[-640.2 \ 74.3 \ -2.1] \text{ km s}^{-1}$ in GSE coordinates. The scatter plot of $\mathbf{V}' (= \mathbf{V} - \mathbf{V}_{HT})$ versus \mathbf{V}_A is shown in Figure 2(b), and is referred to as a Walén plot. The predicted slope of Method 1 by linear regression fitting is pretty close to 1 ($\mathbf{V}'/\mathbf{V}_A = 1.009$), with a correlation coefficient $\gamma_c = 0.992$. The component-by-component scatters of \mathbf{V}' and \mathbf{V}_A from Method 2 are plotted with the $\mathbf{V}_{HT} = [639.5 \ 74.1 \ -2.1] \text{ km s}^{-1}$ in Figure 2(c), which is close to the value derived from Method 1. The linear regression fitting equation of electric field E_c versus E_{HT} by method E1 shows a error (1.670) as seen in Figure 2(d) that is slightly larger than method 1 (0.736) as seen in Figure 2(a). This means the residual electric field from method E1 is not the minimum, but the results of the Walén test are reasonable as found by comparing Method 1 and Method 2. Differing from the above two methods, Method E1 provides a time-varying velocity of the HT frame, which changes slowly during the period, with a quasi-monotonic pattern as shown in Figure 2(e). The three components of \mathbf{V}_{HT} in GSE coordinates manifest as the ambient solar wind moves through the layer structure; generally, the components have a declining trend, as seen in Figure 2(e). Figure 2(f) shows that both the Walén slope and the correlation coefficient are closer to 1, with values of 1.002 and 0.994, respectively, which are slightly better than method 1. Meanwhile, the slopes of the x and z components are

close to 1, but the y component is a little small at 0.744, which shows the poor correlation of V_y and V_{Ay} relative to the x and z components. That is possibly caused by some complex structures in the solar wind stream, with nonmonotonic variation of V_{HTy} . This implies that the velocity components show different degrees of coincidence for the Walén relation. Additionally, other Alfvénic parameters are shown in the top left corner in Figure 2(b), (c) and (f), including the Alfvén ratio γ_A , the normalized cross helicity σ_c , the normalized residual energy σ_R , and the mean deviation E_{π} . These parameters from Method E1 are all improved relative to Method 1 and Method 2, with γ_A (from 1.338 to 1.158) and σ_c (from 0.851 to 0.882) changing closer to 1, and σ_R (from 0.145 to 0.073) and E_{π} (from 0.253 to 0.235) changing closer to 0. In Table 2, the correlation coefficient γ_c , the ratio of SDs $\sigma_{V'_i}/\sigma_{V_{Ai}}$, and the equivalent Walén slope $\gamma_c \frac{\sigma_{V'_i}}{\sigma_{V_{Ai}}}$ from the three methods are listed for comparison, and most of them are optimized by Method E1.

The test results of Cases 2–4 are shown in Figures 3–5, corresponding to Tables 3–5 with the same format as Case 1, respectively. For Case 2, the Alfvénic parameters are more accurate than those of Case 1 overall. Significant Alfvénicity is embodied in the strong correlation ($\gamma_c \geq 0.95$) between \mathbf{V}' and \mathbf{V}_A , as well as the slope and ratio of deviations close to 1. All of the Alfvénic parameters are optimized slightly by Method E1, namely γ_A , σ_c , σ_R , and E_{π} , compared to the results of Method 1 and Method 2. The three components of a time-varying velocity of an HT frame are evaluated by Method E1 with each monotonic trend (an upward trend for V_{HTx} and V_{HTy} , and a downward trend for V_{HTz} , as shown in Figure 3(e)).

For Case 3, the Walén relation is not satisfied very well (the Walén slope is 0.672) though γ_c is high, up to 0.986 in Method 1. That means the conditions of the solar wind stream are complicated and it may be more appropriate to analyze it with a non-constant HT frame. Thus, the Walén tests are conducted in a time-varying HT frame (as shown in Figure 4(e)) determined by Method E1 and produce the scatter diagram seen in Figure 4(f). In Table 4, the ratio $\frac{\sigma_{V'_i}}{\sigma_{V_{Ai}}}$ obtained by Method E1 is optimized from 0.682 up to 0.990, and the Walén slope is optimized from 0.672 up to 0.984. It is clear that, comparing with Method 1 and Method 2, in Method E1 it is preferable to satisfy \mathbf{V}' and \mathbf{V}_A with the Walén relation.

For Case 4, the velocity and magnetic fluctuations correlate quite well for a long interval over 2 hr, with a γ_c of 0.996 and Walén slope of 0.912 for Method 1, as seen in Figure 5(a). Similar to the results for Case 2, using method E1 a monotonous HT frame is found that changes slowly with time, as seen in Figure 5(e). In the time-dependent HT frame, \mathbf{V}' and \mathbf{V}_A satisfy the Walén relation, with a slope of 0.976 and ratio $\frac{\sigma_{V'_i}}{\sigma_{V_{Ai}}}$ of 0.980. Other parameters, including γ_A , σ_c , σ_R , and E_{π} , are close to values from Method 1 and Method 2, as seen in Figure 5(f) and Table 5.

3.3. Walén Test on Difference Data

Without considering the HT frame, two methods can be applied for the modified Walén test, the CHYL method (Method 3) and the second EEMD method (Method E2). According to Chao et al. (2014), for Method 3, five-point smoothing is used to eliminate the high-frequency noises as a low-pass filter before generating the time difference data ΔV and ΔV_A .

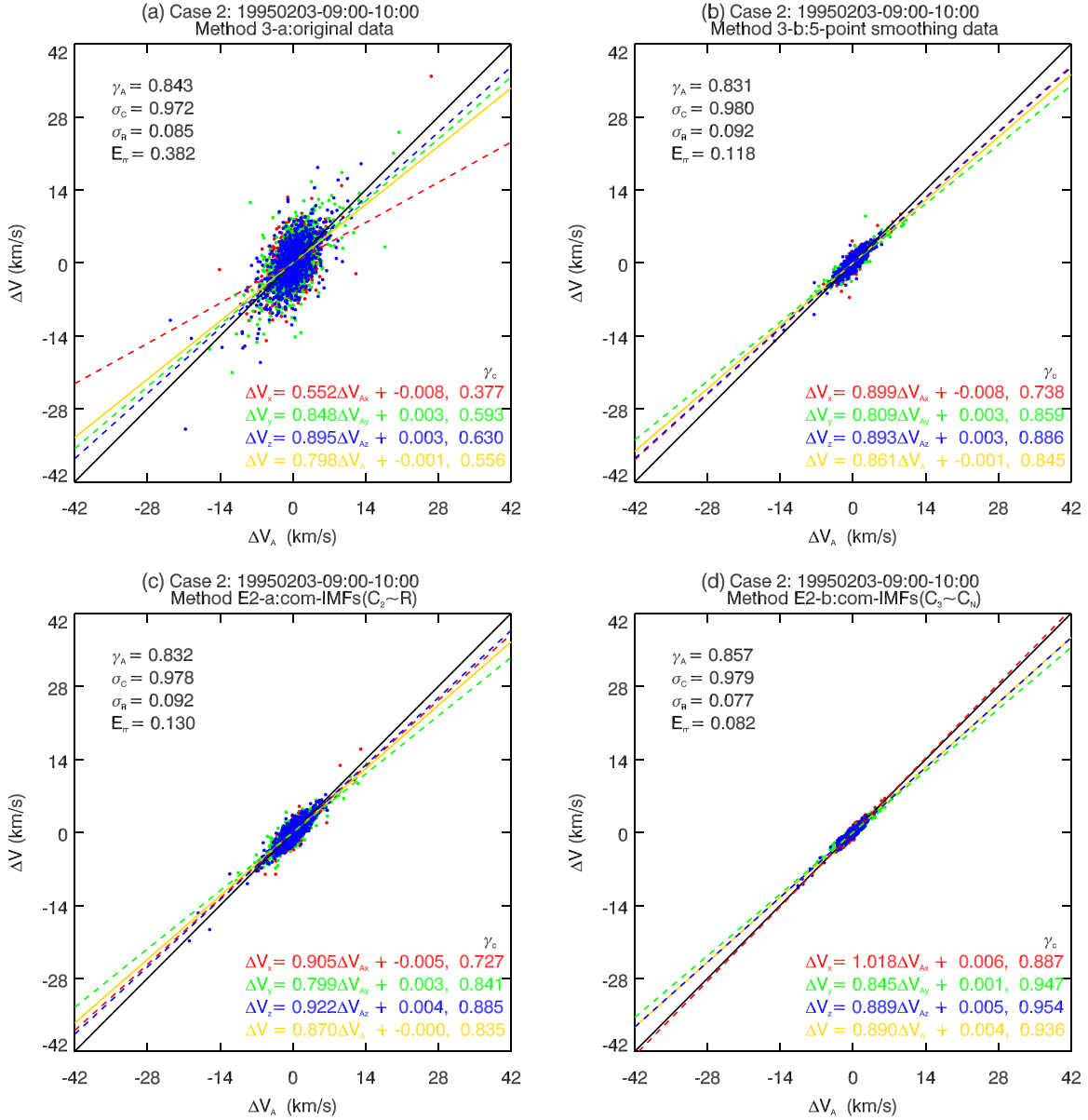


Figure 8. Modified Walén test results of Case 2 in the same format as Figure 7.

In Method E2, we run the EEMD program to deal with components of V and V_A for the same four cases mentioned in Section 3.1. First, setting $N = 100$ and $\alpha = 0.2$. The IMFs of each component decomposed by EEMD are plotted from top (high-frequency) to bottom (low-frequency) in Figure 6. Among them, the high-frequency components (e.g., C_1 , C_2) are mixed with noises from the original data or the random white noises of the EEMD process, while the low-frequency components (e.g., C_{n-1} , C_n , R) probably contain the variation of background field and the HT frame. It can be seen that each IMF of V_i and V_{Ai} corresponds in phase at a very high degree of correlation, especially for the medium-frequency IMFs. The next step is to reconstruct velocity fluctuations by removing some high or low-frequency irrelevance IMFs (residue). Here, in order to determine the IMF combination, we made lots of attempts, such as $C_2 \sim R$, $C_3 \sim R, \dots, C_n \sim R$, $C_2 \sim C_n$, $C_3 \sim C_n, \dots, C_{n-1} \sim C_n$, or $C_2 \sim C_{n-1}$, $C_3 \sim C_{n-1}, \dots, C_{n-2} \sim C_{n-1}$. We found that $C_3 \sim C_n$ is the most optimal combination; according to the Walén slope it is closest to 1. In this process, we treat the

reconstructed IMF components (their sum) as Alfvénic fluctuations for a modified Walén test without considering high-frequency noises and the variation of background fields. The approach with EEMD, just like an adaptive filter, effectively reduces the influences of Alfvénic irrelevant components and the uncertainty from the time-dependent HT frame.

In the results for Case 1, the amplitudes of fluctuations, ΔV and ΔV_A , are plotted and fitted with linear regression equations in Figure 7 for the modified Walén test. The test results and other Alfvénic parameters are shown in the same format used in Figure 7(a)–(d), corresponding to Method 3-a (original data), Method 3-b (five-point smoothing data), Method E2-a (the sum of IMF C_2 to R), and Method E2-b (the sum of IMF $C_3 \sim C_n$), respectively. The reconstructed Alfvénic fluctuations have smaller amplitudes than the original data, similar to the five-point smoothing data. Noticeably, Method E2-b not only optimizes the Walén slope (from 0.986 to 1.007) and the ratio $\frac{\sigma \Delta V_i}{\sigma \Delta V_{Ai}}$ (from 1.780 to 1.176), but also improves the correlation

Table 7
Alfvénic Parameters for the Modified Walén Test of Case 2

Parameter		$\gamma_c \frac{\sigma \Delta V_i}{\sigma \Delta V_{Ai}}$	γ_c	$\frac{\sigma \Delta V_i}{\sigma \Delta V_{Ai}}$
ΔV versus ΔV_A	Method 3-a	0.798	0.556	1.435
	Method 3-b	0.861	0.845	1.019
	Method E2-a	0.870	0.835	1.042
	Method E2-b	0.890	0.936	0.951
ΔV_x versus ΔV_{Ax}	Method 3-a	0.552	0.377	1.464
	Method 3-b	0.899	0.738	1.218
	Method E2-a	0.905	0.727	1.245
	Method E2-b	1.018	0.887	1.148
ΔV_y versus ΔV_{Ay}	Method 3-a	0.848	0.593	1.430
	Method 3-b	0.809	0.859	0.942
	Method E2-a	0.799	0.841	0.950
	Method E2-b	0.845	0.947	0.892
ΔV_z versus ΔV_{Az}	Method 3-a	0.895	0.630	1.421
	Method 3-b	0.893	0.886	1.008
	Method E2-a	0.922	0.885	1.042
	Method E2-b	0.889	0.954	0.932

Table 8
Alfvénic Parameters for the Modified Walén Test of Case 3

Parameter		$\gamma_c \frac{\sigma \Delta V_i}{\sigma \Delta V_{Ai}}$	γ_c	$\frac{\sigma \Delta V_i}{\sigma \Delta V_{Ai}}$
ΔV versus ΔV_A	Method 3-a	0.951	0.678	1.403
	Method 3-b	0.930	0.870	1.068
	Method E2-a	0.960	0.867	1.107
	Method E2-b	0.909	0.891	1.020
ΔV_x versus ΔV_{Ax}	Method 3-a	0.966	0.688	1.404
	Method 3-b	0.956	0.852	1.122
	Method E2-a	0.955	0.828	1.153
	Method E2-b	0.983	0.902	1.090
ΔV_y versus ΔV_{Ay}	Method 3-a	0.588	0.556	1.058
	Method 3-b	0.809	0.818	0.989
	Method E2-a	0.845	0.832	1.016
	Method E2-b	0.889	0.883	1.007
ΔV_z versus ΔV_{Az}	Method 3-a	1.117	0.725	1.541
	Method 3-b	0.949	0.890	1.066
	Method E2-a	0.990	0.891	1.111
	Method E2-b	0.888	0.889	0.999

coefficient (from 0.554 to 0.856), compared with Method 3-a. At the same time, γ_A (from 1.338 to 1.156), σ_c (from 0.851 to 0.871), σ_R (from 0.145 to 0.072), and E_{tr} (from 0.446 to 0.153), are improved as seen in Figure 7(a) and (d). The Alfvénic parameters of the x , y , z components from the two methods are listed in Table 6. γ_c and $\frac{\sigma \Delta V_i}{\sigma \Delta V_{Ai}}$ of all three components are significantly improved, especially for ΔV_x versus ΔV_{Ax} . The Alfvénic parameters obtained by Method E2-b are closer to 1 (or 0) than those obtained by Method 3 and E2-a.

The results of the modified Walén test of Case 2, Case 3, and Case 4 are shown in Figures 8–10 and Table 7–9 with same format as Figure 7 and Table 6, respectively. For Case 2, γ_c (from 0.556 to 0.936) and the Walén slope (from 0.798 to 0.890) are closer to 1, as obtained by Method E2-b, relative to Method 3-a. There are few changes in γ_A (from 0.843 to 0.857), σ_c (from 0.972 to 0.979), and σ_R (from 0.085 to 0.077),

Table 9
Alfvénic Parameters for the Modified Walén Test of Case 4

Parameter		$\gamma_c \frac{\sigma \Delta V_i}{\sigma \Delta V_{Ai}}$	γ_c	$\frac{\sigma \Delta V_i}{\sigma \Delta V_{Ai}}$
ΔV versus ΔV_A	Method 3-a	0.966	0.734	1.316
	Method 3-b	0.927	0.921	1.007
	Method E2-a	0.949	0.915	1.037
	Method E2-b	0.941	0.962	0.978
ΔV_x versus ΔV_{Ax}	Method 3-a	0.866	0.683	1.268
	Method 3-b	0.902	0.901	1.001
	Method E2-a	0.928	0.886	1.047
	Method E2-b	0.917	0.955	0.960
ΔV_y versus ΔV_{Ay}	Method 3-a	0.929	0.736	1.262
	Method 3-b	0.942	0.927	1.016
	Method E2-a	0.946	0.919	1.029
	Method E2-b	0.962	0.961	1.001
ΔV_z versus ΔV_{Az}	Method 3-a	1.047	0.760	1.378
	Method 3-b	0.929	0.927	1.002
	Method E2-a	0.962	0.929	1.035
	Method E2-b	0.940	0.967	0.972

and obvious optimization in E_{tr} (from 0.382 to 0.082), as seen in Figures 8 (a) and (b). Compared with Method 3-b, Method E2-b achieved a higher correlation coefficient, with values of 0.936, 0.887, 0.947, and 0.954 for the velocity vector and x , y , z components, respectively, which are also higher than that of method E2-a. $\frac{\sigma \Delta V_i}{\sigma \Delta V_{Ai}}$ values are improved by Method E2-b, with values from 1.435 to 0.951 relative to Method 3-a in Table 7. Moreover, Method E2-b has a minimum value of both σ_R and E_{tr} among the results of modified Walén tests.

For Case 3, Method E2-a produces a Walén slope with a value of 0.960, which is close to 1, and Method E2-b produces an optimal $\gamma_c = 0.891$ [0.902, 0.883, 0.889], $\frac{\sigma \Delta V_i}{\sigma \Delta V_{Ai}} = 1.020$ [1.090, 1.007, 0.999] for the velocity vector and components, respectively. However, in terms of Figure 9, neither Method 3-b nor Method E2 improve the values of γ_A , σ_c , σ_R , except for E_{tr} (from 0.292 to 0.068). The kinetic energy density is less than the magnetic energy density with a ratio of 0.530 ~ 0.626, and the normalized residual energy is greater than 0.250.

For Case 4, the slopes are high, with values of 0.966, but γ_c are not so high, with values of 0.734 of unfiltered ΔV versus ΔV_A , as seen in Figure 10(a). The correlation coefficients rise up to 0.962 [0.955, 0.961, 0.967] for velocity vector and x , y , z components, respectively, by Method E2-b. The ratios $\frac{\sigma \Delta V_i}{\sigma \Delta V_{Ai}}$ are quite close to 1 (1.007 [1.001, 1.016, 1.002]) of the smoothed difference data from Method 3-b, as shown in Table 9. The values of γ_A , σ_c , σ_R have few changes from Method 3-a, from Method 3-b to Method E2-a, and from Method E2-b, while E_{tr} is improved from 0.253 to 0.031 by Method E2-b.

4. Discussions

Four cases of Alfvénic fluctuations in high-speed solar wind are studied in this work. There are strong correlations between the observed plasma velocity and magnetic fluctuations ($\gamma_c > 0.9$) in all four cases, but their amplitudes match to different degrees. The slopes of their least-squares regression are not stationary, which represents the ratio of $(V - V_{HT})$ versus V_A . In order to obtain better and more stationary slopes, two

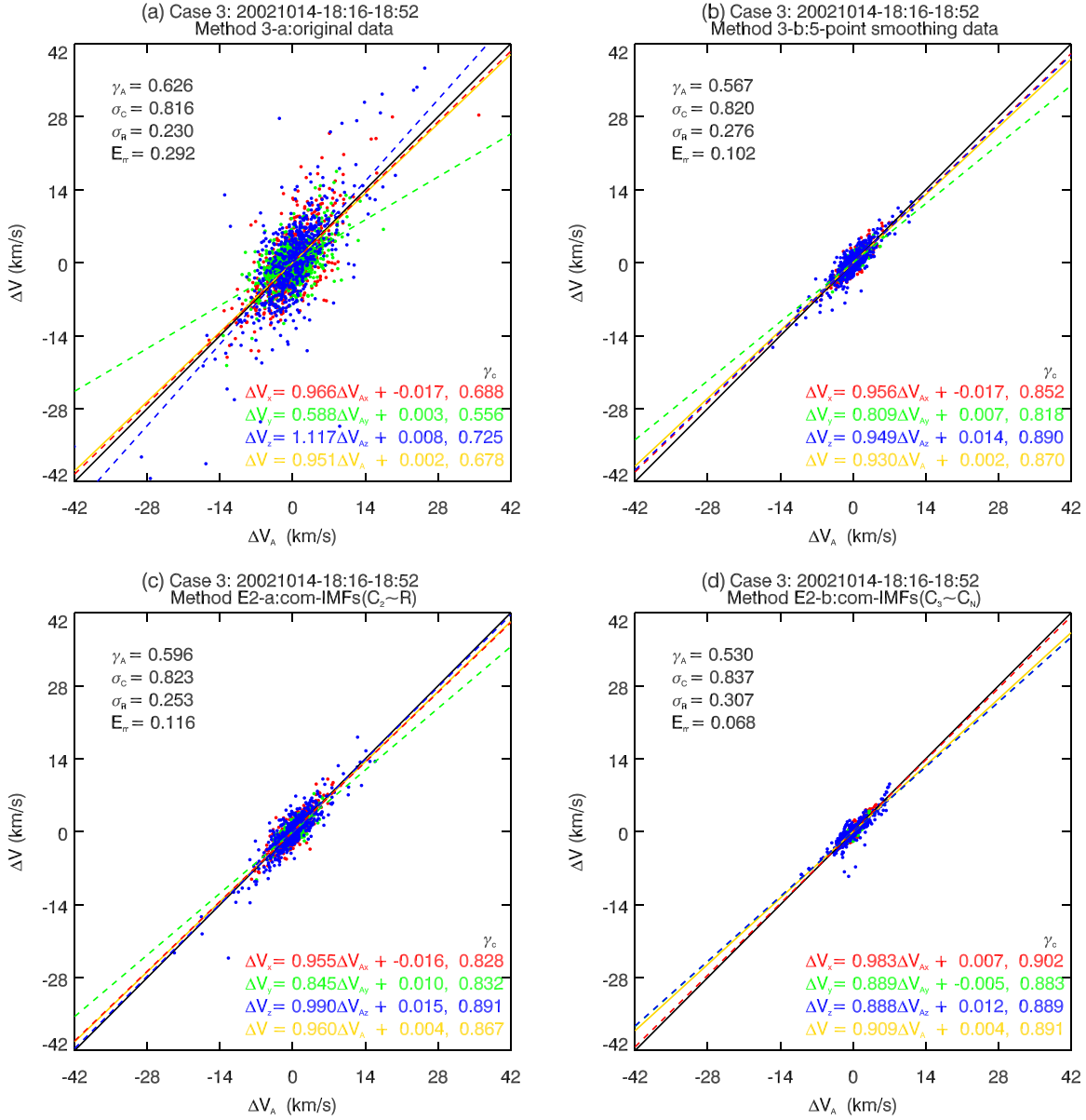


Figure 9. Modified Walén test results of Case 3 in the same format as Figure 7.

different approaches are executed for the Walén test of plasma and magnetic fluctuations during the periods of four cases.

On the one hand, the conventional Walén test based on the HT frame is carried out by three methods (Method 1, Method 2, and Method E1) in Section 3.2. A few different Walén slopes are obtained from Method 1 and Method 2, concretely, the slopes of V' versus V_A in Case 1, Case 2, and Case 4 are closer to 1 (>0.9), while the slope of Case 3 is away from 1. In comparison with Method 1 and Method 2, in which the time series are checked under a constant HT frame, Method E1 makes the Walén slopes and the ratios $\frac{\sigma V'_i}{\sigma V_{Ai}}$ closer to 1 by evaluating a time-varying HT frame. Other Alfvénic parameters also are optimized by Method E1, such as γ_A , σ_c , σ_R , and E_σ .

We found that the Walén relation is better satisfied by fluctuations for the trailing portion of the stream (Case 2 and Case 4) than the leading stream (Case 1 and Case 3), although the correlations between fluctuations of magnetic field and velocity are very close to 1 in each case. It is generally

considered that this is possibly due to the influence of strong compression at the leading of high-speed streams. However, the Walén slopes and ratio $\frac{\sigma V'_i}{\sigma V_{Ai}}$ obtained by method E1 are significantly closer to 1 than those for Method 1 and Method 2 in Case 1 and Case 3. This indicates the importance of evaluating the proper HT frame for the Walén test. Additionally, the regression slopes of the x , y , z components are quite different for all three methods, which may be a potential problem for deeper and more comprehensive research on Alfvénic fluctuations with discontinuous structures.

On the other hand, the time difference data of V and V_A are analyzed in the modified Walén test by the CHYL methods (Method 3-a and Method 3-b). The only difference between these two methods is that the former uses the original data while the latter uses the five-point smoothed data. The slopes from the original data are almost close to 1 ($\gamma_c \frac{\sigma \Delta V_i}{\sigma \Delta V_{Ai}} > 0.95$), while the ratios of deviations ΔV_i versus ΔV_{Ai} are significantly

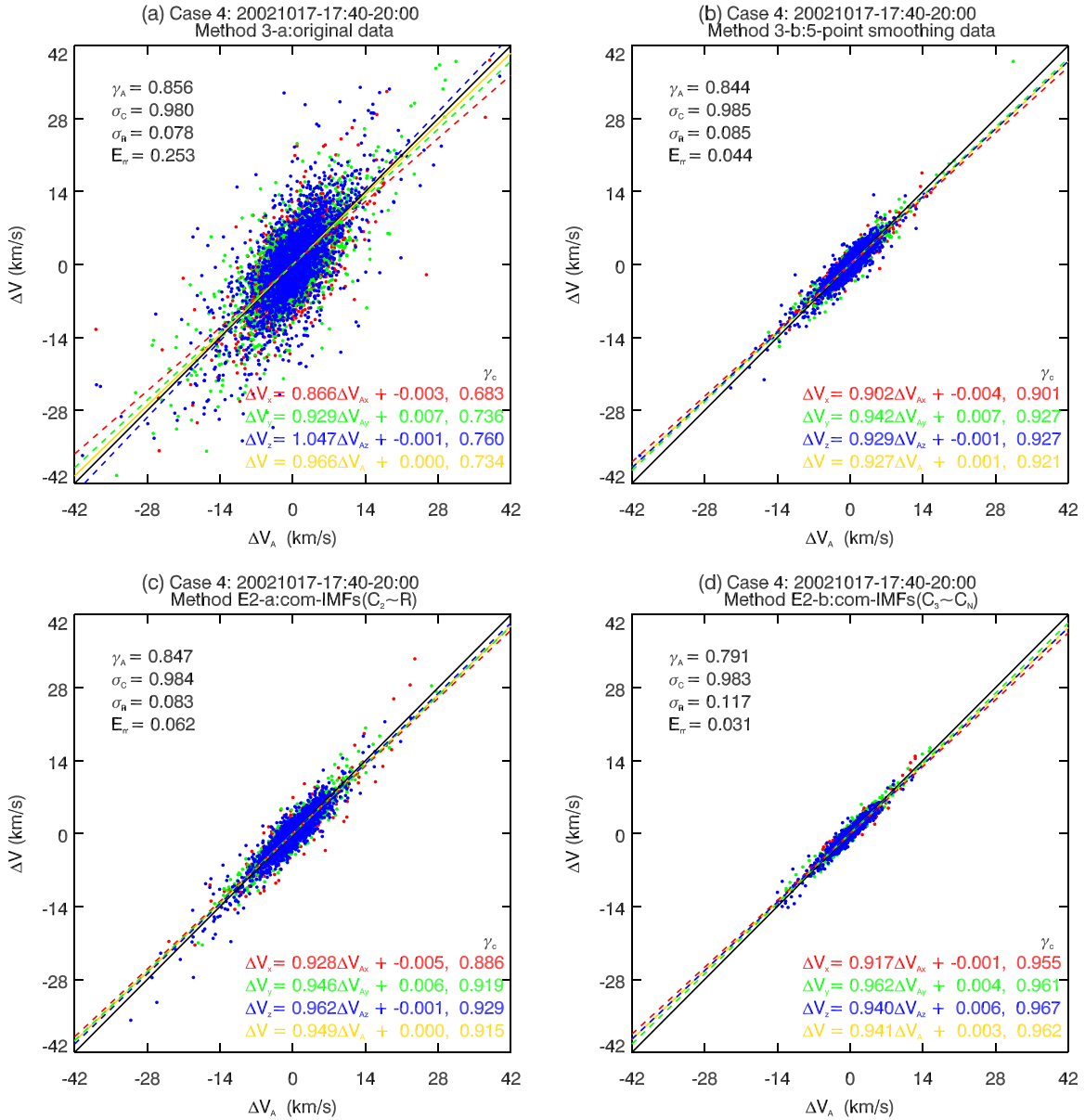


Figure 10. Modified Walén test results of Case 4 in the same format as Figure 7.

greater than 1, and the correlation coefficients of ΔV_i and ΔV_{A_i} are relatively low, with values of about 0.5 ~ 0.7. If smoothing data improve these Alfvénic parameters, this likely is due to high-frequency components irrelevant to Alfvénicity. Specifically, the amplitudes of the high-frequency components are reduced and the results from Method 3-b are obviously closer to 1 than those of Method 3-a, which uses smoothed data. There is some artificiality in choosing the filter band for smoothing. In Section 3.3, the EEMD methods (Method E2-a and Method E2-b) are applied for the modified Walén test using different IMF combinations as the reconstructed Alfvénic fluctuations. Compared with the CHYL methods, the IMF group of $C_2 \sim R$ presents results almost similar to those from the five-point smoothed data, but the IMF group of $C_3 \sim C_N$ produces the optimal Alfvénic parameters substantially, especially the correlation coefficients and the ratios of deviations. This means that EEMD can efficiently eliminate high-frequency components and vary the background from the original observation, which is irrelevant for Alfvénic

fluctuation. As a result, the time differences of the IMF groups from EEMD are more likely suitable for the modified Walén test, even for Case 3 with a more complex HT frame. These comparisons demonstrate that Method E2-b can be used for the modified Walén test as effectively as Method 3, by virtue of the significant affect on noise reduction and superior Alfvénic parameters.

We would like to point out that more fluctuations need to be considered to analyze the robustness of EEMD methods, especially for complex scenarios such as spikes or large-amplitude discontinuous structures existing in the selected period.

5. Conclusions

AFs are common physical phenomena in solar wind streams, with a distinctive feature in which the fluctuations of plasma velocity and magnetic field are parallel and proportional to each other in observations. But there are some uncertainties in

identifications of Alfvén waves based on single-satellite observations at 1 au. This is not only due to the contamination of other propagating waves and non-propagating magnetic structures, but also because of errors caused by data processing.

The Walén relation, as a criterion for identifying Alfvén waves, is usually tested in a constant HT frame where the local solar wind plasma is coherent with an interplanetary magnetic field in a steady medium. But a constant HT frame may be invalid in some complex cases, such as when there is a time-dependent or multiple HT frame (Gosling et al. 2009). Considering this, Alfvén waves also can be identified through a modified Walén test using time difference data in the CHYL method (Chao et al. 2014), regardless of the HT frame and other uncertainties. This method can be used to identify the Alfvén waves better, using smoothed data.

In this article, we propose a new Walén test based on self-adapting data analysis technology, the EEMD method, which is intended to analyze the nonlinear and nonharmonic data. In the EEMD process, an (ensemble) average decomposition of signals adds finite-amplitude white noise that is treated as IMFs, and the original data are decomposed into a series of IMFs and a monotonous residual. For comparison, the EEMD process is performed in two ways: the first way is a conventional Walén test based on the HT frame (Method E1); the other is a modified Walén test independent of the HT frame (Method E2).

Parameters related to Alfvénicity are calculated for comparison between different methods, including the Walén slope, correlation coefficient γ_c , ratio of the deviations $\frac{\sigma V_i}{\sigma V_{Ai}}$ or $\frac{\sigma \Delta V_i}{\sigma \Delta V_{Ai}}$, and the Alfvén ratio γ_A , the normalized cross helicity σ_c , the normalized residual energy σ_R , and the average of the SD ratio E_{tr} . Except for σ_R and E_{tr} , which need to be as close to 0 as possible, the other parameters mentioned above imply purely Alfvén waves if they are very close to 1. Four cases of large-amplitude Alfvénic fluctuations are analyzed based on single-satellite (*WIND*) observations in a high-speed solar wind stream.

For the conventional Walén test, we extract a time-dependent HT frame from the decomposed residual of the plasma and Alfvén velocity deviation ($V_i - V_{Ai}$) via EEMD. It is found that Method E1 has superior Alfvénicity. Most of the parameters are optimized, closer to 1 than is seen for the methods with a constant HT frame, while σ_R and E_{tr} are closer to 0 as expected.

In the modified Walén tests, it is found that the high-frequency components and slow variation of the background that are unrelated to Alfvénicity can be naturally eliminated from the original data via EEMD. Using the reconstructed fluctuations of the plasma velocity and Alfvén velocity (combinations of IMFs), Method E2 obtains results similar to those of the CHYL method using the smoothed data. And method E2 is more flexible due to its use of the selected IMFs obtained from EEMD. Most of the Alfvénic parameters for the four studied cases are optimized, except for σ_c and σ_R , which occasionally get a little bit worse.

In summary, according to the results for the four cases studied in this article, we provide an new and alternative approach to the Walén test for identifying Alfvén waves in solar wind: the self-adapting EEMD technique. The EEMD method not only evaluates a time-dependent HT frame velocity, but also produces a higher degree of Alfvénic parameters in either the conventional

or modified Walén test. There will be more applications for EEMD for Alfvénic fluctuation observations in the future, due to its ability to decompose and reconstruct nonstationary signals in the time-frequency domain. Furthermore, the reconstructed fluctuations from EEMD have detailed local properties in narrow frequency bands, which have rarely been discussed before, making it possible to better understand the physical essence of Alfvénic fluctuations in the solar wind.

This work was supported by the National Nature Science Foundation of China (grants No. 41664008 and 41574167) and the Funds from the Key Laboratory of Space Weather, National Center for Space Weather, China Meteorological Administration. The authors thank the teams of *WIND* mission and OMNI database and the CDAWEB for access to the data needed for this study. We are grateful to the research center for adaptive data analysis of National Central University for the free code of EEMD. We also thank Dr. Lei Yang for providing useful discussions and suggestions.

ORCID iDs

Jin Liu  <https://orcid.org/0000-0002-1757-8285>

ChuanBing Wang  <https://orcid.org/0000-0001-6252-5580>

References

- Alazraki, G., & Couturier, P. 1971, *A&A*, **13**, 380
- Alberti, T., Consolini, G., Lepreti, F., et al. 2017, *JGRA*, **122**, 4266
- Alfvén, H. 1947, *MNRAS*, **107**, 211
- Barnes, A., & Hollweg, J. V. 1974, *JGR*, **79**, 2302
- Barnes, F. L., Bollman, W. E., Curkendall, D. W., & Thornton, T. H. 1962, MARINER 2 FLIGHT TO VENUS, Tech. Rep. JPL-TR-32-395 (Pasadena, CA: Jet Propulsion Lab., California Inst. of Tech.), <https://ntrs.nasa.gov/search.jsp?R=19630003720>
- Belcher, J. W., & Davis, L., Jr. 1971, *JGR*, **76**, 3534
- Belcher, J. W., Davis, L., Jr., & Smith, E. J. 1969, *JGR*, **74**, 2302
- Bruno, R., Bavassano, B., & Villante, U. 1985, *JGR*, **90**, 4373
- Burlaga, L. F. 1971, *SSRv*, **12**, 600
- Carbone, F., Gencarelli, C. N., & Hedgecock, I. M. 2016a, *PhRvE*, **94**, 063101
- Carbone, F., Landis, M. S., Gencarelli, C. N., et al. 2016b, *GeoRL*, **43**, 7751
- Chao, J. K., Hsieh, W.-C., Yang, L., & Lee, L. C. 2014, *ApJ*, **786**, 149
- Coleman, P. J. J. 1967, *P&SS*, **15**, 953
- De Hoffmann, F., & Teller, E. 1950, *PhRv*, **80**, 692
- De Pontieu, B., McIntosh, S. W., Carlsson, M., et al. 2007, AAS Meeting Abstracts, **210**, 94.15
- Eisenhauer, J. G. 2003, *Teaching Statistics*, **25**, 76
- Flandrin, P., Rilling, G., & Gonçalves, P. 2004, *ISPL*, **11**, 112
- Carbone, F., Sorriso-Valvo, L., Alberti, T., et al. 2018, *ApJ*, **859**, 27
- Gosling, J. T., McComas, D. J., Roberts, D. A., & Skoug, R. M. 2009, *ApJL*, **695**, L213
- He, J. S., Tu, C.-Y., Marsch, E., et al. 2009, *A&A*, **497**, 525
- Huang, N. E., Shen, Z., Long, S. R., et al. 1998a, *RSPSA*, **454**, 903
- Huang, N. E., Zheng, S., & Long, S. R. 1998b, *AnRFM*, **31**, 417
- Huang, Y. X., Schmitt, F. G., Lu, Z. M., & Liu, Y. L. 2008, *EL*, **84**, 40010
- Hudson, P. D. 1971, *P&SS*, **19**, 1693
- Jacques, S. A. 1977, *ApJ*, **215**, 942
- Jensen, E. A., Nolan, M., Bisi, M. M., Chashei, I., & Vilas, F. 2013, *SoPh*, **285**, 71
- Khrabrov, A. V., & Sonnerup, B. U. Ö. 1998, *ISSIR*, **1**, 221
- Lepping, R. P., Acuña, M. H., Burlaga, L. F., et al. 1995, *SSRv*, **71**, 207
- Li, H., Wang, C., Chao, J. K., & Hsieh, W. C. 2016, *JGRA*, **121**, 42
- Lin, R. P., Anderson, K. A., Ashford, S., et al. 1995, *SSRv*, **71**, 125
- Marsch, E., & Richter, A. K. 1984, *JGR*, **89**, 5386
- Martínez-Sykora, J., Pontieu, B. D., Hansteen, V. H., Voort, L. R. V. D., & Pereira, T. M. D. 2017, *Sci*, **356**, 1269
- Matthaeus, W. H., & Goldstein, M. L. 1982, *JGR*, **87**, 6011
- Matthaeus, W. H., Zank, G. P., Oughton, S., Mullan, D. J., & Dmitruk, P. 1999, *ApJL*, **523**, L93
- Mavromichalaki, H., Moussas, X., Quenby, J. J., et al. 1988, *SoPh*, **116**, 377

- McIntosh, S. W., de Pontieu, B., Carlsson, M., et al. 2011, [Natur](#), **475**, 477
- Paschmann, G., & Daly, P. W. 2000, Analysis Methods for Multi-Spacecraft Data (Noordwijk: ESA)
- Sonnerup, B. U. O., & Cahill, L. J. J. 1967, [JGR](#), **72**, 171
- Sonnerup, B. U. O., Papamastorakis, I., Paschmann, G., & Luehr, H. 1987, [JGR](#), **92**, 12137
- Tomczyk, S., McIntosh, S. W., Keil, S. L., et al. 2007, [Sci](#), **317**, 1192
- Tsurutani, B. T., & Gonzalez, W. D. 1987, [P&SS](#), **35**, 405
- Tu, C. Y., & Marsch, E. 1995, MHD Structures, Waves and Turbulence in the Solar Wind: Observations and Theories (Dordrecht: Kluwer)
- Unti, T. W. J., & Neugebauer, M. 1968, [PhFl](#), **11**, 563
- Walén, C. 1944, [ArMAF](#), **30A**, 1
- Wang, C. B., Wang, B., & Lee, L. C. 2014, [SoPh](#), **289**, 3895
- Wang, X., He, J., Tu, C., et al. 2012, [ApJ](#), **746**, 147
- Wentzel, D. G. 1974, [SoPh](#), **39**, 129
- Wu, C. S. 1995, [PhST](#), **60**, 91
- Wu, Z., & Huang, N. E. 2004, [RSPSA](#), **460**, 1597
- Yang, L., & Chao, J. K. 2013, [ChJSS](#), **33**, 353
- Yang, L., Lee, L. C., Chao, J. K., et al. 2016, [ApJ](#), **817**, 178
- Yokoi, N., & Hamba, F. 2007, [PhPl](#), **14**, 112904